Using Aerial Morphology to Enhance Safety and Efficiency of Unmanned Aerial Systems

Ronald Whiting
Florida Polytechnic University
Computer Science
Dr. Dean Bushey

December 8, 2016

1 Abstract

The future of aviation is moving toward complete autonomy; Corporations are pursuing permissions to operate unmanned aerial systems (UAS) in the National Airspace System (NAS) under semi-autonomous to full autonomous control, and an increase in the number of UAS being used by civilians in the private sector necessarily means that the skies are soon to be densely populated with these systems. One way to accommodate the increasingly high population of UAS in the NAS is to improve the efficiency of the flight paths of these systems. These flight paths involve either altering the distance of separation (FAA regulated) or improving the detection of the system to avoid and take positive evasive action from potentially dangerous objects while detecting, but not necessarily navigating away from the benign objects. The goal is to increase efficiency of the sense and avoid detection system while maintaining safety by positively determining the threat level of an aerial object. Dangerous aerial threats include manned aerial vehicles, while benign aerial threats include aerial biologicals. These are classified as benign because of their capacity for agile movements and curious/protective nature over their territory. Using Boolean Image multiplication to distinguish various aerial objects, we were able to obtain a confidence level of 99.847% that there is a noticeable difference between the aerial objects using steady state analysis. These differentiations are stepping stones toward an enhanced Detect, Sense, and Avoid system using morphological analysis to increase efficiency.

Contents

List of Figures

List of Tables

2 Introduction

The importance of detect, sense, and avoid subsystems in unmanned aerial system(UAS) is the safe and efficient operation of UAS in the National Airspace System(NAS) is becoming increasingly critical. This study focuses on the improvement in detection ability of non-cooperative sense and avoid and detect, sense, and avoid systems. The non-cooperative sense and avoid system is a system that can be entirely contained onboard a UAS giving it the capability to remain a safe distance from other airborne aircraft and avoid collision. This improvement of the ability to classify aerial objects helps the integration of UAS into the NAS through flight path efficiency, which can potentially increase the capacity for UAS in the NAS. The increase in flight path efficiency is attained through the classification of threat levels, which may allow for a much more passive flight path adjustments to deal with benign threats. Aerial biological objects are considered benign aerial threats due to their natural maneuverability and their protective curiosity of foreign aerial objects in their territory. The study examines the differentiation between manmade biological aerial objects. The classification of aerial objects is achieved through time varying morphological analysis using Boolean image multiplication. Throughout the discussion and suggestions of the topic of non-cooperative UAS sense and avoid systems, many incremental improvements have been introduced to make the integration of UAS into the NAS possible. Initial systems gave Boolean responses due to the presence of any aerial objects in the host UAS field of view [9] [10] to the current stages of the systems tracking objects and calculating collisions [14] [15]. Research into a system that will comply with the high density of UAS using the ability to calculate and omit non-threatening aerial objects is the next logical iteration.

This study will present data showing the ability of Boolean image multiplication to classify an aerial object as a manmade or biological object. The contribution to sense and avoid subsystem is improved efficiency through classification of dangerous versus benign aerial threats.

3 Background

The popularity of unmanned aerial systems among the population of the United States is rising significantly every year [9, 16]. UAS hold enormous promise for our economy and for the aviation industry. But for the industry to develop to its full potential, we have to ensure that it develops safely [9]. The technology is becoming easier to acquire and use. Due to the high volume of unmanned aerial system sales and the high number of untrained users, UAS began to unintentionally intrude the NAS potentially creating hazardous environments for authorized traffic. "Air traffic control (ATC) received increasing reports of unauthorized and unsafe use of small UAS. Pilot reports of UAS sightings in 2015 are double the rate of 2014. Pilots have reported seeing drones at altitudes up to 10,000 feet, or as close as half-a-mile from the approach end of a runway" [9]. The safety of the National Airspace System prompted the Federal Aviation Administration to create restrictions [2–4,9,15] and a registration system [2,3,9,15] and to prepare a complete set of regulations [1,5,14,16] for these unmanned aerial systems.

The personal and commercial potential of this disruptive technology was recognized by corporations, civilians, and the government [9, 15]. The price of the technology in comparison to equivalent manned equipment is significant and the ever-widening variety of the functions the technology can be applied to could not be ignored [9, 15]. Corporations and government are pressing for the expedient establishment of the regulations, to be granted the authorization to use these unmanned aerial systems as powerful assets. The establishment of the regulations was the initial step towards the safe use of UAS in the NAS. Difficulty arose with the resulting hazard branching from the inability for an unmanned system to avoid collisions with other aircraft, which resulted in the call for a Sense and Avoid capability [1,3,14,16]. Sense and avoid capability means the capability of an unmanned aircraft to remain a safe distance from and to avoid collision with other airborne aircraft [3].

Sense and avoid capability exists and is currently in use aboard airlines and high-end aircraft. The current sense and avoid capable technologies in use are cooperative avoidance systems (TCAS and ADS-B); cooperative avoidance means that the avoidance systems work together by broadcasting their location and trajectory to other cooperative avoidance systems in the area calculating and alerting the crew members on a possible collision path [1,14]. The ADS-B and TCAS sense and avoid technologies have a native weakness, the nature of cooperative systems [1,10,11]. Cooperative avoidance systems can only sense and avoid other cooperative avoidance systems. These cooperative avoidance systems are not required by law to be used by the entire population of the NAS, which makes unequipped aircraft invisible to the current systems and requires periodic human monitoring. Secondary complications with the system that limit its full integration into the population of the NAS include its cost, weight, size, and power consumption [1, 8, 10, 11]. This prompted research into a sense and avoid capable system that could be used with non-cooperative systems.

The evolution of the non-cooperative sense and avoid started with a Boolean search and avoidance response. The system detected an object in the field of view of the sensor and immediately avoided the object [6,14,17]. This initial step proved that the system was responsive. Improvements were further studied and implemented to sense the depth and size of the object detected. This improvement used the comparison of the size of the aerial object to the size of the host unmanned aerial system to send an indication to the avoidance system that the object should be avoided [14,17]. This improvement modestly explored the threat level of aerial objects based on size. The threat based solely on size is unsatisfactory, as UAS, birds, and aircraft come in many different sizes and forms [7].

The next iteration of improvements incorporates the trajectory of the detected aerial object. The size (referenced to host UAS), depth, and trajectory of the object are correlated with the velocity of the host unmanned aerial systems and the sense system calculates the potential for a collision given the two objects (host UAS and foreign object) present course [8, 10–12]. This iteration of improvement explores the size (relative to self) and trajectory as a level of threat. This system has the potential to avoid a collision of an object with steady heading and attitude, but the potential for an object to rapidly change the direction in all the sky is high and the process is computation intensive. The sense and avoid systems development then started pivoting towards hybrid systems that analyze a fusion of sensors to improve the accuracy of the system in different environmental situations by comparing resulting data about the aerial object detected [8,13]. The fusion studies focus on the abilities of multiple sensors for their variety of strengths to offset the weaknesses of the other sensors. This sensing fusion was used to improve abilities in low light scenario and visibly inconvenient weather conditions. The advantage of using a system of checks and balances is the increased accuracy.

The exploration of the research of sense and avoid systems has brought several improvements; the under researched areas are the over sensitivity in the sense systems to aerial objects, the inability to handle rapidly maneuvering aerial objects, and the foresight to understand the complications that a highly-populated airspace introduces for this type of system.

4 Methodology

Sense and Avoid Identification System

The SAA Identification System (See Appendix A) will be a system that incorporates stereoscopic and aerial morphological identification to produce a hybrid system yielding greater results in efficiency and accuracy for UAS flight paths and object classification. The Boolean indication of an object from the stereoscopic subsystem activates the morphological subsystem (See Appendix A: Morphological Identification). The hybrid system will use the counterbalancing influences from the subsystems to further verify the SAA identification systems final decision.

Morphological Identification

Morphology identification use inverse background subtraction. The goal is to find the foreground object and its steady state in contrast to the transient portions of the centered aerial object. The foreground object full unprocessed primary profile is averaged with the secondary frames object profile and given a ratio based against the objects processed steady state profile. This ratio equals the area of the objects steady state over the averaged full profile of the object. The bias threshold was found based upon test data. The concept is the morphology of an aerial biological fluctuates far more rapidly than typical manmade aerial vehicles during active thrust and lift.

Morphology of a manmade aircraft contrast to an aerial biological, are much steadier. The more notable parts of a fixed wing aircraft are the wings and the fuselage which remain stationary in relation to the entire profile. The noticeable transient portion of the fixed wing aircraft is its propeller for its constant motion. The aliased propeller captured in the video stream is smaller compared to the main components of its profile. A rotorcraft body profile is identified through its main rotor and fuselage. The aliased main rotor captured in the video stream is small in comparison with its fuselage. The aerial biological is set apart by its organic movements and motions. Aerial biologicals are commonly identified through the motion of their wings. The motions and movements of the aerial biological contrasted with traditional manmade vehicles are appreciably evident. Manmade aerial objects maintain a higher steady state profile area despite various methods of thrust and lift compared to aerial biologicals.

The experimental platform uses a computer workstation and open source computer vision software to test the hypotheses in this study. The computer workstation is a 64-bit Ubuntu 16.04 linux based computer work station equipped with Python 2.7 and Open Source Computer Vision(OPENCV) 3.0 with python equipped libraries. The completed SAA identification system (outside of this study) is designed to run on an ARM core unix-based Raspberry Pi 3 Model B microcomputer with integrated Raspberry Pi NOIR Rev.1.3 cameras. In order to stay within the parameters of the physical hardware of the completed system a unix-based computer was utilized for the duration of the study. The open source computer vision software used in the study also has been experimentally tested and found to work with the linux-based microcomputer. The experimental platform uses systems and programming that have the ability to be directly transferred to the microcomputer upon completion of the system.

The replication of the study involves a simulated object tracking, noise reduction, and binary thresholding. Each sample is a grayscale image of a single aerial object with a light blue region as background centered in the video stream as if object tracking is being applied. The maintained centering of the object in the video stream is mandatory for overlay in the process of Boolean image multiplication. Boolean image multiplication uses time varying frames from the video stream to yield the steady state profile.

Noise reduction is accomplished through image smoothing, which uses a 5x5

Gaussian normal distribution to eliminate the noise from the background. Noise in the video stream includes darker areas and undesirable visibility of clouds, particles in the sky, and very fine details that would show unwanted variations in the illumination of the foreground aerial object.

Binary thresholding is a technique that applies a replacement of pixel value (intensity) to 255 (white) or 0 (black) depending on the state of the original pixel value as above or below a pixel threshold. This process is used to further illuminate the aerial object by providing higher contrast to the video stream frames. The binary threshold is used to separate the foreground object from the background sky region.

The featured process in this study is Boolean image multiplication process, which calculates the steady state ratio. The steady state ratio is a ratio calculated from the steady state profile of the aerial object over the time duration in which the frames were acquired (seen in Equation 1)

$$SSP = r_g^1(t) \times \frac{r_g^2(t')}{r_{gmax}} \tag{1}$$

and the average area of the full profile of the aerial object from the interval varying frames used in the process (seen in Equation 2).

$$SSR = \frac{SSP_{Area}}{\overline{FP_{Area}}} \tag{2}$$

The Area of the objects steady state is acquired and a ratio is created between the area of the steady state to the average area of the entire signal at the two different time periods. The ratio calculated in the process is used to classify the object through the amount of change in its structure while maintaining active thrust and flight. The ratio calculated from the objects morphology is then correlated to either aerial biological object or aerial manmade object separated by a bias threshold.

Hypothesis

Null Hypothesis (H_0): There will be no change between the steady state ratios of the manmade versus the Steady State Ratios of the aerial biological objects.

Alternative Hypothesis (H_A): There will be a directional change between the steady state ratios of the manmade versus the Steady State Ratios of the aerial biological objects.

The Hypothesis used to define the study is searching for a change in the groups of video sample frames that shows a significant difference in the manmade aerial objects from the aerial biological objects.

$$H_0 : SSR_M \leq SSR_B$$
$$H_A : SSR_M > SSR_B$$

The quantitative research model was used to research the differentiation of the aerial objects. The steady state ratios were directly relatable to the question of distinguishing objects through their morphology by the mean values of each dataset(Aerial Biological and Aerial Manmade). The statistical analysis chosen to decipher whether a change could be measured is the Heteroscedatics One-tailed Paired T-test. The

One-tailed paired t-test is a statistical tool used to analyze the mean differences between datasets to determine whether one dataset is significantly greater than another.

Using Boolean image multiplication an outcome can only come from the significant difference in the steady state ratios created from the video sample subjects. The assumption that a manmade aerial object has a higher steady state ratio than an aerial biological object is used in the hypothesis to gain further depth into the understanding of the resulting probability and application.

The data sets used in the study were acquired from Instagram footage. There were 399 steady state ratios collected from the process of Boolean image multiplication. 21 different variations of frames were used in each video sample. 19 video samples of aerial objects at 30 fps (.033s between frames) were chosen for the study. 252 steady state ratios were collected from all variations of corresponding video samples pertaining to aerial biologicals. 147 steady state ratios were collected in all frame variations from corresponding video samples that contain manmade aerial objects. Due to the unequal variability of the datasets, a Heteroscedastic Paired T-test is required.

There are limitations of this model system. This study is the preliminary work toward improvements to the SAA and DSA system with the respect to threat avoidance efficiency. The current limitations of the system are the ability to process and identify only one object per frame, against a background of a light blue region unobstructed by landscape. The ability to detect based on the size of the bird due to the surface area of the wing and the frequency needed to keep the biological aloft. This method is limited to biologicals actively providing thrust; soaring or gliding observed through the system may not accurately be classified correctly. The system is limited by the intensity of the hue of the aerial objects; any aerial objects emitting (color or reflectivity) intensities analogous to the sky region may be filtered out as noise.

This study assumes that the video stream sample aerial biological object represents all aerial biological objects. The sample objects used in the study as manmade vehicles span only fixed wing aircraft and single main/tail rotor rotorcraft. The intensity of the hue of both manmade and biological objects are assumed to be a lower magnitude than the hue intensity of the sky region backdrop. The study only looks at aerial objects located in the main forward facing field of view to be perceived as either a chase object or an object approaching head-on. The objects flight path is assumed to be steady straight and level flight.

5 Results

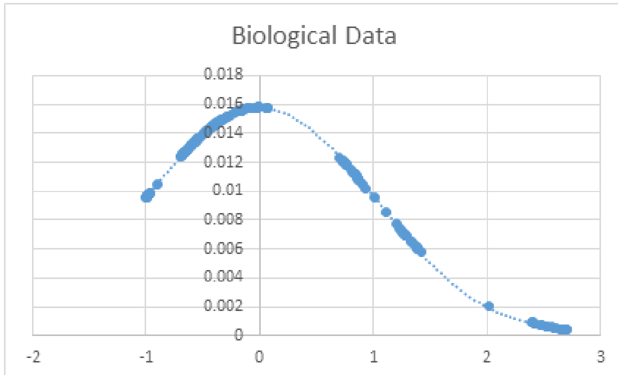

Table 1: Aerial Biological Object Data (Standard Normal Distribution)

Biological Data					
μ-3σ	μ-2σ	μ-σ	μ+σ	μ+2σ	μ+3σ
0	1	184	23	23	21
		82.14285714			
	91.66666667				
100					
Mean: 25.879					
Std Dev: 25.223					

Table 2: Aerial Object Biological Data Interpretation (Standard Deviation Percentiles)

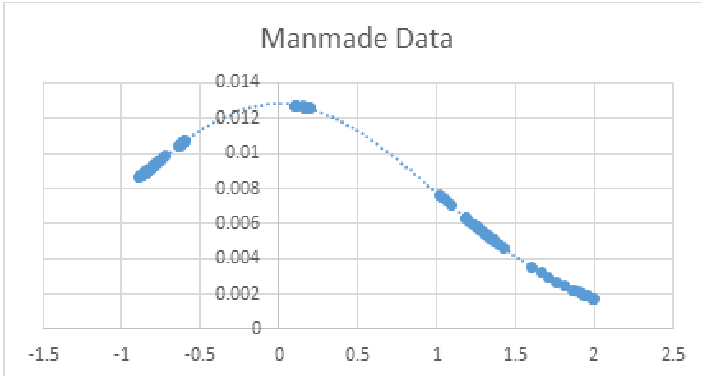

Table 3: Aerial Manmade Object Data (Standard Normal Distribution)

Manmade Data					
μ-3σ	μ-2σ	μ-σ	μ+σ	μ+2σ	μ+3σ
0	0	84	21	41	1
		71.42857143			
	99.31972789				
100					
Mean: 34.952					
Std Dev: 31.192					

Table 4: Aerial Manmade Object Data Interpretation (Standard Deviation Percentiles)

The Heteroscedastic Paired T-test between the aerial biological and manmade objects' steady state ratios yielded a P-value of 0.001524.

Biological Bias Threshold Data					
μ-3σ	μ-2σ	μ-σ	μ+σ	μ+2σ	μ+3σ
0	1	184	23	23	21
		82.14285714			
	91.66666667				
100					
Mean: 25.879					
Std Dev: 25.223					
Bias Threshold Accuracy 30.41 (.179 Std):					0.25

Table 5: Aerial Biological Object Bias Threshold Differentiation Accuracy (%)

Manmade Bias Threshold Data					
μ-3σ	μ-2σ	μ-σ	μ+σ	μ+2σ	μ+3σ
0	0	84	21	41	1
		71.42857143			
	99.31972789				
100					
Mean: 34.952					
Std Dev: 31.192					
Bias Threshold Accuracy 30.41(-.1456 Std):					0.503401

Table 6: Aerial Manmade Object Bias Threshold Differentiation Accuracy (%)

The differentiation accuracy found in this study from the bias threshold in the two data sets yielded a 25% accuracy rate for the aerial biological objects and 50.3

6 Discussion

The T-test produced an outcome of P-value = 0.001524. The data shows the confidence level in the discernibility of aerial objects is 99.847%. The data proved that the detection of an aerial biological from manmade vehicles is possible and could warrant further study and analysis using this and related techniques. The two data sets are normalized to prepare and clarify which type of T-test statistical analysis is needed for the data points. The normalized data shows that the variances are not matched and a heteroscedastic (different variabilities) one-tail T-test is needed. Observation of the normal distribution curve tells us that the mean of the data sets are different and a good candidate for the T-test analysis.

This study representing the initial work conducted with aerial morphology identification the default was chosen as it is universally accepted. A default significance level of 5% was used. This study represents the initial work conducted with aerial morphology identification thus this was selected.

The system's lower level process test, yielding the steady state profile confirms the theory of isolating the steady state portions of the aerial objects. The aerial biological profile experiences notable clipping around the wing tips during the ornithological motion the wings undergo. The steady state profile of the body of the aerial biological remains almost untouched as it is present in all motions that the aerial objects morphology.(As seen in Figure below)

The steady state profile of an aerial manmade object also confirms the theoretical argument of the manmade aerial object and corresponding ratio maintaining the majority of its normal operating profile. As seen in figure below, the majority of

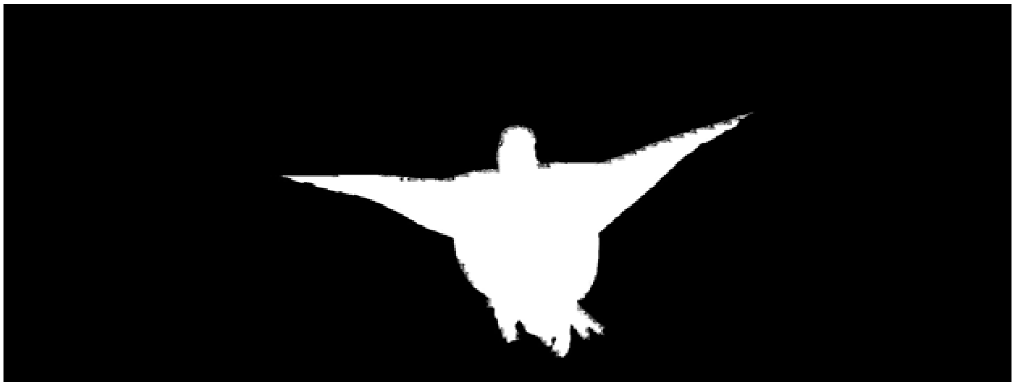

Figure 1: Steady State Aerial Biological Profile from Aerial Biological Video Sample: 4 (Left/Right Transient Wing Portions Clipped)

the profile is complete confirming the steady state nature of manmade aerial objects, the small variations in the profile are due to transient portions as well as some noise experienced from the difference in position from one frame to the next.

Sources of errors in the study in respect to Boolean image multiplication include

Figure 2: Steady State Aerial Manmade Object Profile from Rotorcraft Video Sample: 2 (Steady State Portion Remains)

errors in position centering, thresholding. The ability of the system to keep the aerial object centered is essential to the boolean image multiplication process. The aerial object must overlay as cleanly as possible in order to yield the most accurate profile. The thresholding used in this study is a binary threshold that operates under a fixed value. Changes in lighting and object color may cause errors to occur. The reflectivity of the object due to sunlight and color of the object can be incorrectly transformed, which results in inaccurate aerial object profiles.

The T-test analysis of the data sets resulted in a P-value = .001524. The P-value shows the probability that a random value will occur. The corresponding 99.847% confidence level is found in the results. The P-value and the confidence level suggest that there is strong evidence against the null hypothesis, resulting in the rejection of the null hypothesis. The Alternative hypothesis is accepted.

The statistical analysis T-test is a powerful statistical test. The problem with the T-test under the conditions that exist in the study are the quantity of the data. The T-test is said to require all points in studies under 15 data points to make a perfect normal distribution with no outliers. The T-test is less stringent for data sets of 40 and above, the test is said to be strong even when data is skewed beyond the distributed curve. The nonequivalent number of points in data sets are said to be valid, but the absent data points could represent the additional resolution of the data not seen otherwise. The absence of additional data points and resolution has the possibility to create a type I error of a false positive.

The Alternative Hypothesis has been accepted and reveals the outcome of this study. The secondary question is if there is a bias threshold, can it be located and used to make the differentiation between the manmade aerial objects and the aerial biological objects. The mean values of the standard normal distributions previously calculated are used in the selection of the bias threshold. The calculated bias threshold was 30.41. In Table 3 and Table 4, bias threshold show that the bias threshold calculated using the average of the means found in the two data sets. The accuracy of the prediction based on the calculated bias threshold was 25% and 50.3%.

The alternative hypothesis are the focus of this study, preliminary normal distributions of the individual video samples for the question of which frame and frame variation of the data most accurately represents the data. Normal distributions of each video sample data is collected not under any intense scrutiny, but as observation data and a courtesy to researchers continuing the study. Based on a snapshot of the data (See Appendix B), the time variation of my results in relation to the average, 73.53% of the steady state ratio remained within a single standard deviation of the average. Further analysis is needed into the effects of time variation of frames on the steady state ratio.

7 Conclusion

In conclusion, I have used this methodology to prove that given the data set and strength of the test there is a possibility that distinguishing between aerial manmade objects and aerial biological objects. Using Boolean image multiplication, I was able to produce data to indicate steady state ratios may be used in categorical classification of aerial objects to identify aerial biological objects from manmade aerial objects. The system has the potential to increase flight path efficiency by granting the ability of identifying and omitting benign aerial threats. Supplementary effects of flight path efficiency may include improvements in energy and time efficiency as well as extending UAS vehicle lifespan longevity and each deserve further study in the wake of the current study.

8 Future Work

The results and process of this study have lead to theories of possible improvements, newly discovered directions to further advance the study, and promising interesting directions.

The possible steps to move toward to improve the study take place in the process of frame preparation involving noise reduction. The noise being addressed is any portion of the object in the frame that isn't clearly perceived by the boolean image multiplication as seen in Figure 3.

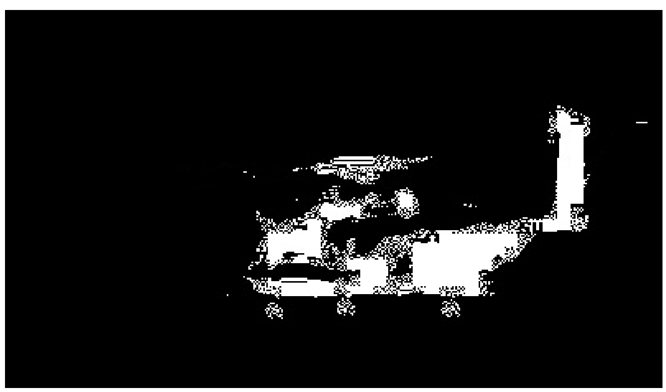

Figure 3: Aerial Manmade Object Profile from Rotorcraft Video Sample: 3 (Noise produced from object contrast during thresholding process)

Further clarification of noise include inaccuracies in complete profiles of aerial objects. This noise is caused by high contrast within the object due to the suns reflection, the inability to actively change the threshold in which the binary segmentation occurs, and the inability to automatically center the aerial object from one time interval to the next (more accurate overlay for boolean image multiplication) within the frame (full frame or selected area). The introduction of histogram equalization and adaptive thresholding in the preparation of the frames would decrease the contrast of the original frame eliminating shadows and glares on the object that would have a significant effect on the object profile. An active object tracking to substitute the simulated object tracking in the study should be used in future studies. The use of an automatic system for this purpose allows for a wider range of samples and more reliable data collection.

The results of the study yielded new questions which are closely related to the advancement in the efficiency of the aerial morphological subsystem. The determination of whether an ideal frame time interval exist that would accurately embody the steady state ratio of the entire aerial object. The possibility of there existing more than one ideal frame time interval cooresponding to the altitude that the aerial object is currently located. The existence of an ideal frame time interval would decrease amount of data required to be collected to distinguish between aerial objects and subsequently the amount of processing power needed to achieve the ultimate goal of aerial object differentiation.

The new method that arose as a possible promising path of aerial object differentiation is morphological rate of change. Using specific lengthier contours of an aerial objects profile the rate of change in the shape of the contour is measured to identify the object, this method operates under the similar assumption that the rate of change of an aerial biological object is higher than an aerial manmade object, which presumably would have a small rate of change along its lengthier contours. The contours would be more efficiently detected with a high pass filter with less pixels to account for

9 Appendix

9.1 Appendix A: Flowchart

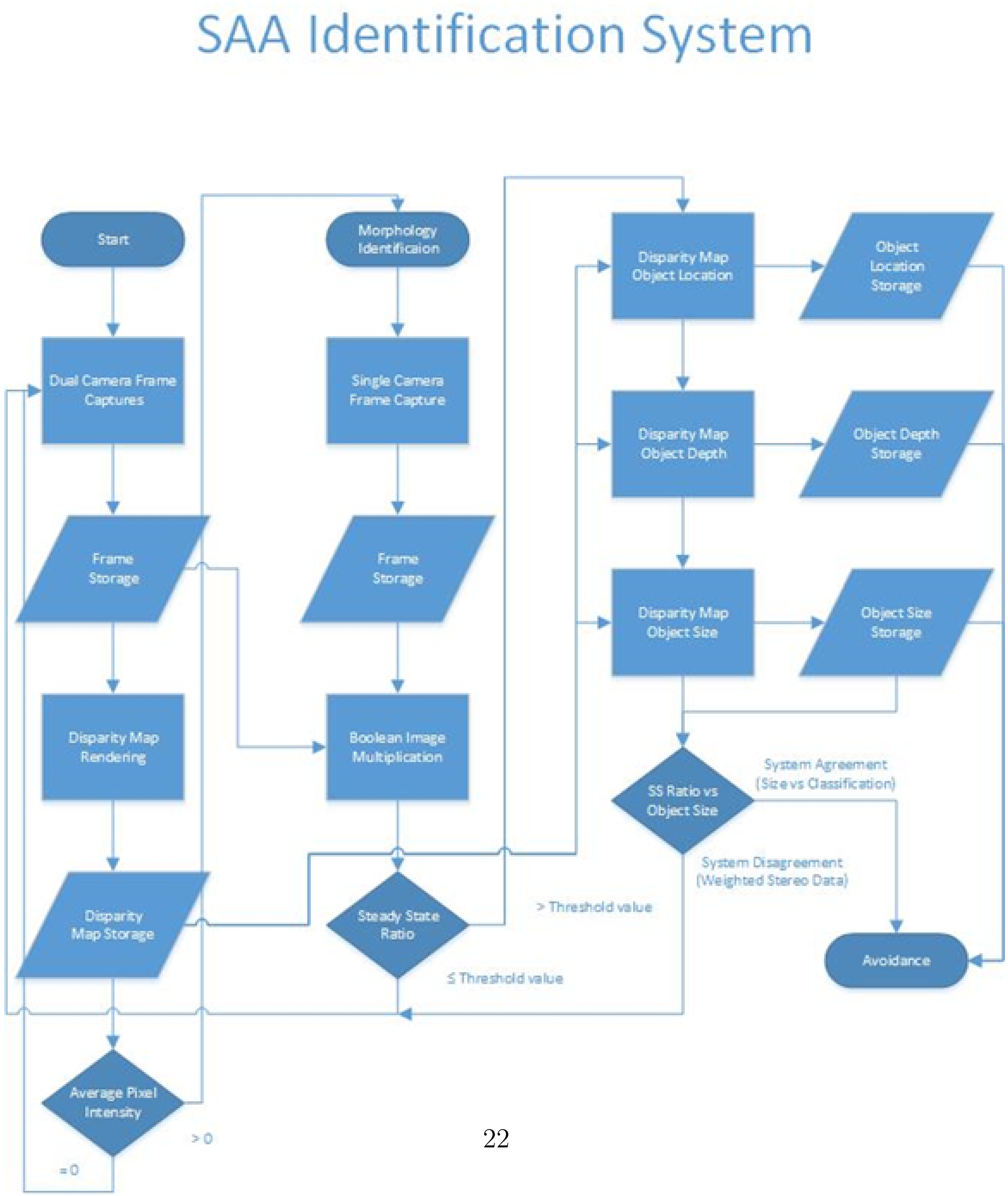

Figure 4: SAA Identification System

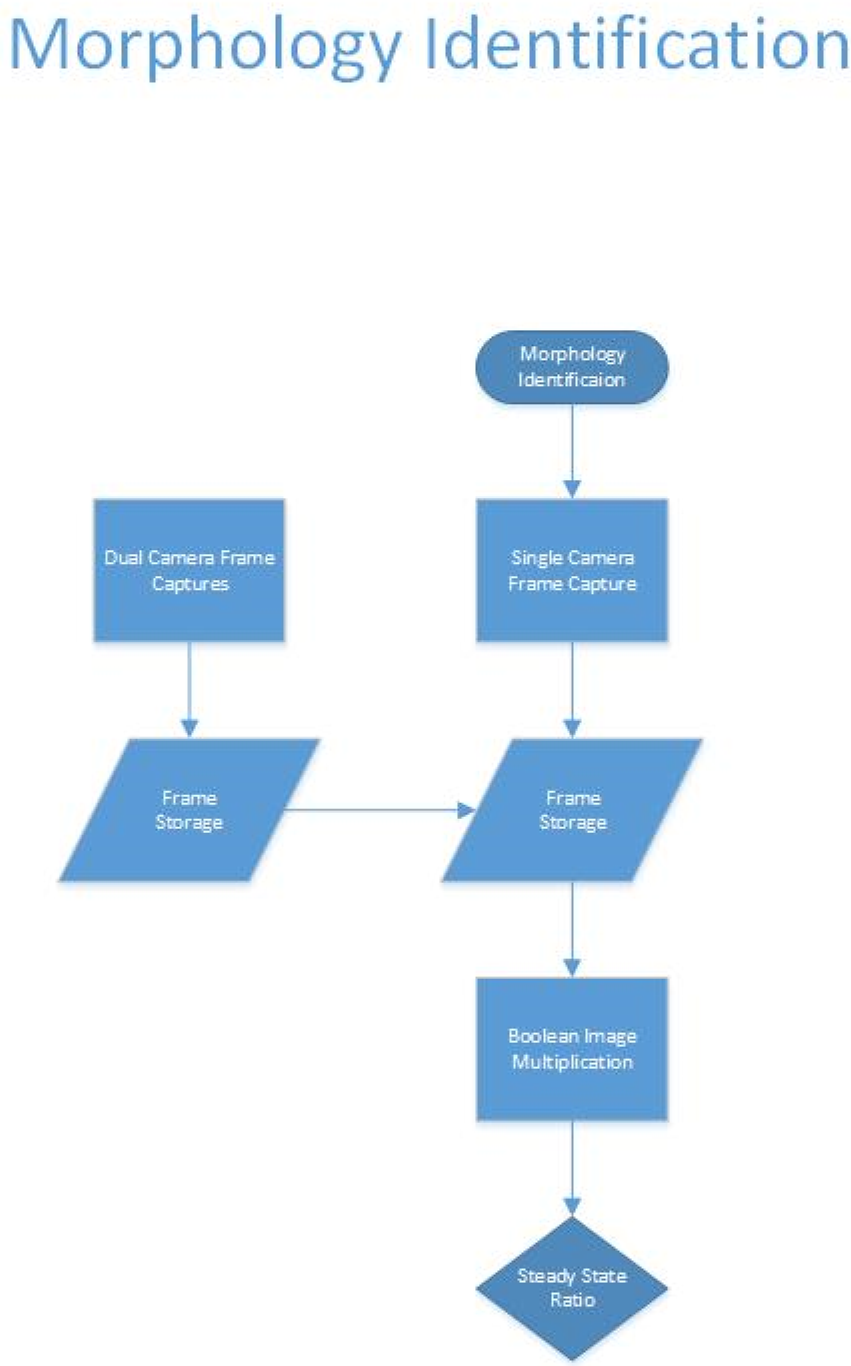

Figure 5: Morphological Identification Subsystem

9.2 Appendix B: Steady State Ratio Data

Frame Variation	Slide0_1	Slide0_2	Slide0_3	Slide0_4	Slide0_5	Slide0_6	Slide1_1	Slide1_2	Slide1_3	Slide1_4	Slide1_5	Slide2_1	Slide2_2	Slide2_3	Slide2_4	Slide3_1	Slide3_2	Slide3_3	Slide4_1
Aerial Object													Fixed Wing Video Sample 1						
Steady State Ratio	0.754898	0.765085	0.775491	0.784162	0.773717	0.770211	0.739053	0.746564	0.766567	0.755658	0.747775	0.734959	0.758913	0.748458	0.741245	0.737101	0.730421	0.724766	0.679591
Steady State Percentage	75.48975	76.50848	77.54915	78.41617	77.37169	77.02112	73.90525	74.65641	76.65669	75.56581	74.77751	73.4959	75.89133	74.84583	74.12454	73.71015	73.04208	72.47657	67.95912
Aerial Object													Fixed Wing Video Sample 2						
Steady State Ratio	0.72094	0.719452	0.796101	0.913792	0.974484	0.95812	0.670164	0.759938	0.899711	0.955646	0.952685	0.723263	0.868827	0.933898	0.970786	0.850209	0.944395	0.93304	0.882303
Steady State Percentage	72.09398	71.94516	79.61006	91.37917	97.44841	95.81199	67.01642	75.99377	89.97114	95.5646	95.26845	72.32633	86.88266	93.38979	97.07863	85.02093	94.43953	93.30403	88.23025
Aerial Object													Fixed Wing Video Sample 3						
Steady State Ratio	0.159455	0.160858	0.160795	0.154468	0.156108	0.157272	0.163378	0.16341	0.156666	0.158407	0.159424	0.163915	0.157486	0.159236	0.160534	0.156992	0.158767	0.159997	0.150935
Steady State Percentage	15.94554	16.08577	16.07949	15.44683	15.61084	15.72723	16.33784	16.34097	15.66661	15.84072	15.94239	16.39145	15.74864	15.92363	16.05342	15.69915	15.87667	15.99975	15.09347
Aerial Object													Fixed Wing Video Sample 4						
Steady State Ratio	0.096723	0.096311	0.097136	0.101388	0.102178	0.103179	0.098103	0.098255	0.102053	0.101922	0.10292	0.100869	0.104372	0.10322	0.104716	0.109164	0.108293	0.110346	0.114716
Steady State Percentage	9.672293	9.631059	9.713568	10.13884	10.21784	10.31789	9.81031	9.825486	10.20527	10.1922	10.292	10.0869	10.43719	10.32203	10.47158	10.91645	10.8293	11.03458	11.47159
Aerial Object													Biological Video Sample 1						
Steady State Ratio	0.24012	0.174156	0.139241	0.134928	0.144347	0.155537	0.208986	0.164123	0.150807	0.152069	0.150515	0.184309	0.161551	0.151496	0.142734	0.169344	0.149453	0.119792	0.149843
Steady State Percentage	24.01199	17.41561	13.92412	13.4928	14.43473	15.55372	20.89864	16.41229	15.08067	15.20691	15.05146	18.43089	16.15514	15.1496	14.27341	16.93438	14.94528	11.97923	14.98425
Aerial Object													Biological Video Sample 2						
Steady State Ratio	0.009589	0.008302	0.00803	0.00803	0.007234	0.006182	0.008907	0.008556	0.008556	0.007838	0.00658	0.013397	0.013397	0.008415	0.006967	0.01357	0.008398	0.007094	0.008398
Steady State Percentage	0.95893	0.83016	0.802995	0.802995	0.723416	0.618226	0.890709	0.855572	0.855572	0.783834	0.657957	1.339676	1.339676	0.84151	0.696737	1.357049	0.839843	0.709366	0.839843
Aerial Object													Biological Video Sample 3						
Steady State Ratio	0.031045	0.010474	0.010498	0.009137	0.010246	0.011577	0.01041	0.010442	0.009105	0.010238	0.011585	0.013959	0.010243	0.010072	0.008922	0.010203	0.010104	0.008921	0.011509
Steady State Percentage	3.104535	1.047441	1.049841	0.913679	1.024577	1.157683	1.040987	1.044193	0.910452	1.023758	1.15849	1.395936	1.024286	1.00721	0.892156	1.020278	1.01041	0.892142	1.150875
Aerial Object													Biological Video Sample 4						
Steady State Ratio	0.154334	0.118278	0.096392	0.088731	0.08589	0.085739	0.147664	0.120177	0.106114	0.098268	0.095814	0.159657	0.135412	0.12044	0.113212	0.18114	0.152544	0.138541	0.193619
Steady State Percentage	15.43341	11.82781	9.639231	8.873081	8.589021	8.573858	14.76638	12.01771	10.61142	9.826808	9.581411	15.96574	13.54117	12.04398	11.32117	18.11404	15.25438	13.8541	19.36195
Aerial Object													Biological Video Sample 5						
Steady State Ratio	0.185978	0.163657	0.155742	0.147467	0.12522	0.107573	0.172463	0.159269	0.143081	0.118953	0.109292	0.163197	0.139166	0.11533	0.104923	0.158842	0.131656	0.114635	0.162771
Steady State Percentage	18.59775	16.36573	15.57423	14.7467	12.522	10.75727	17.24633	15.92695	14.3081	11.89526	10.92917	16.31971	13.91662	11.53296	10.4923	15.8842	13.16565	11.46348	16.27706
Aerial Object													Biological Video Sample 6						
Steady State Ratio	0.575447	0.583049	0.581287	0.595115	0.594397	0.616415	0.570657	0.568732	0.582647	0.583524	0.607781	0.561646	0.575773	0.579106	0.606621	0.567492	0.572795	0.601826	0.579204
Steady State Percentage	57.54468	58.30495	58.1287	59.51149	59.43966	61.64151	57.0657	56.87316	58.26467	58.35243	60.77814	56.16458	57.57732	57.91056	60.66211	56.74921	57.27954	60.18262	57.92043
Aerial Object													Biological Video Sample 7						
Steady State Ratio	0.21904	0.214832	0.21492	0.213789	0.210825	0.211689	0.216622	0.216264	0.214631	0.212026	0.212566	0.222244	0.219428	0.215437	0.216854	0.222189	0.216945	0.218991	0.217691
Steady State Percentage	21.90402	21.48323	21.49199	21.37891	21.0825	21.1689	21.66219	21.62639	21.46307	21.20259	21.25664	22.22442	21.94275	21.54371	21.68537	22.21892	21.6945	21.89908	21.76912
Aerial Object													Biological Video Sample 8						
Steady State Ratio	0.175696	0.165618	0.152261	0.159825	0.157372	0.15093	0.169396	0.156741	0.159789	0.154826	0.15271	0.158854	0.16113	0.155915	0.153305	0.173138	0.165933	0.162276	0.187226
Steady State Percentage	17.56959	16.56179	15.22608	15.98255	15.73716	15.09299	16.9396	15.67411	15.97887	15.48256	15.27099	15.88539	16.11305	15.59155	15.33049	17.3138	16.59329	16.22764	18.7226
Aerial Object													Biological Video Sample 9						
Steady State Ratio	0.254321	0.254542	0.254459	0.254459	0.233325	0.233541	0.169396	0.156741	0.159789	0.154826	0.15271	0.274164	0.274164	0.251066	0.251368	0.274413	0.250838	0.251058	0.250838
Steady State Percentage	25.43206	25.45422	25.4459	25.4459	23.33247	23.35414	16.9396	15.67411	15.97887	15.48256	15.27099	27.41637	27.41637	25.10657	25.13683	27.44134	25.08383	25.10577	25.08383
Aerial Object													Biological Video Sample 10						
Steady State Ratio	0.768319	0.860436	0.863839	0.863938	0.906349	0.894663	0.864153	0.867408	0.867507	0.910237	0.89822	0.886123	0.886123	0.940499	0.929343	0.882561	0.938259	0.926726	0.938303
Steady State Percentage	76.83187	86.0436	86.38388	86.39375	90.63491	89.46628	86.41531	86.74082	86.75073	91.02373	89.82204	88.6123	88.6123	94.04987	92.93429	88.25612	93.82588	92.67263	93.8303
Aerial Object													Biological Video Sample 11						
Steady State Ratio	0.098182	0.096194	0.094081	0.090326	0.087881	0.083202	0.098179	0.096502	0.092402	0.089482	0.083879	0.099826	0.095471	0.095633	0.088643	0.09641	0.096005	0.088706	0.103049
Steady State Percentage	9.818166	9.619404	9.408075	9.032568	8.788078	8.320231	9.817928	9.650155	9.240175	8.948222	8.387942	9.982556	9.547124	9.563309	8.864302	9.64103	9.600527	8.870615	10.30492
Aerial Object													Biological Video Sample 12						
Steady State Ratio	0.539128	0.478316	0.451841	0.436588	0.442233	0.450208	0.494336	0.465275	0.444503	0.45208	0.460724	0.512983	0.472662	0.475843	0.478168	0.487649	0.482137	0.475647	0.469402
Steady State Percentage	53.9128	47.8316	45.18412	43.65882	44.22329	45.0208	49.43364	46.52751	44.45031	45.20799	46.07244	51.29825	47.26616	47.58428	47.8168	48.76487	48.21366	47.56466	46.94018
Aerial Object													Heli Video Sample 1						
Steady State Ratio	0.407735	0.407273	0.410494	0.408192	0.402737	0.381097	0.410366	0.408708	0.405973	0.403315	0.383038	0.409264	0.40563	0.402385	0.383304	0.408896	0.401153	0.380593	0.402079
Steady State Percentage	40.77353	40.72728	41.0494	40.81923	40.27374	38.10969	41.03658	40.87083	40.59732	40.33148	38.30376	40.92639	40.56299	40.23852	38.33044	40.88962	40.1153	38.0593	40.20787
Aerial Object													Heli Video Sample 2						
Steady State Ratio	0.089449	0.08449	0.08241	0.077295	0.081703	0.083325	0.086386	0.084755	0.078881	0.082467	0.085345	0.086534	0.079567	0.083326	0.085243	0.081921	0.085054	0.087122	0.084611
Steady State Percentage	8.944878	8.449033	8.241038	7.729479	8.170262	8.332549	8.638586	8.475493	7.888096	8.246736	8.534509	8.653387	7.956702	8.33264	8.524286	8.192131	8.505417	8.712161	8.461099
Aerial Object													Heli Video Sample 3						
Steady State Ratio	0.080338	0.076453	0.073281	0.07756	0.072152	0.082468	0.084823	0.079609	0.082238	0.076485	0.087599	0.084307	0.085483	0.078304	0.0888	0.088869	0.07934	0.089833	0.080713
Steady State Percentage	8.033817	7.645274	7.328119	7.755952	7.215169	8.246757	8.482265	7.960937	8.223801	7.6485	8.759891	8.430713	8.548331	7.830385	8.880041	8.886933	7.934014	8.983274	8.071284

Figure 6: Steady State Ratio Data

Slide4_2	Slide5_1	Mean	Variance	Standard Deviation
0.690336	0.66789	0.742517	0.000957	0.030932971
69.03365	66.78901			
0.959703	0.97052	0.874189	0.010083	0.100413015
95.97034	97.05199			
0.151964	0.152616	0.158223	1.3E-05	0.003605036
15.19638	15.26163			
0.11756	0.125451	0.104708	5.46E-05	0.00738855
11.75601	12.54509			
0.114694	0.143356	0.15721	0.000782	0.027969952
11.46943	14.33562			
0.007094	0.00738	0.008663	4.68E-06	0.002163768
0.709366	0.737984			
0.009261	0.012331	0.011442	2.17E-05	0.004653581
0.926128	1.23313			
0.166602	0.203748	0.131539	0.001294	0.035969638
16.66021	20.37477			
0.136362	0.159921	0.14169	0.000569	0.023856068
13.63624	15.99212			
0.608255	0.607312	0.586623	0.000259	0.016080649
60.82553	60.73119			
0.218811	0.230643	0.216973	1.99E-05	0.004456239
21.88111	23.0643			
0.163447	0.167665	0.162098	8.01E-05	0.008951138
16.34472	16.76648			
0.251058	0.272137	0.232343	0.00191	0.043702117
25.10577	27.21373			
0.92677	0.91833	0.892291	0.001587	0.039832927
92.67695	91.83301			
0.094791	0.103755	0.093933	3.11E-05	0.005576101
9.47913	10.37549			
0.445165	0.469762	0.470698	0.000609	0.024679517
44.5165	46.97621			
0.380275	0.3971	0.399981	0.000122	0.011030214
38.02749	39.70998			
0.089267	0.090908	0.084289	1.19E-05	0.003443147
8.926656	9.090814			
0.090676	0.098128	0.082736	4.1E-05	0.006405527
9.06763	9.812771			

Figure 7: Steady State Ratio Data

9.3 Appendix C: Aerial Object Time Interval Data

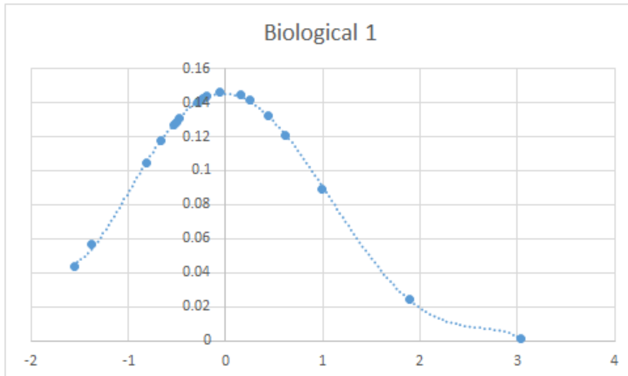

Figure 8: Aerial Biological Object Video Time Interval SND: Sample One

Standard Deviation Percentage					
μ-3σ	μ-2σ	μ-σ	μ+σ	μ+2σ	μ+3σ
0	2	12	5	1	0
0	0.1	0.6	0.25	0.05	0
0	10	60	25	5	0
		85			
	100				
100					

Figure 9: Aerial Biological Object Time Interval Video Interpretation: Sample One

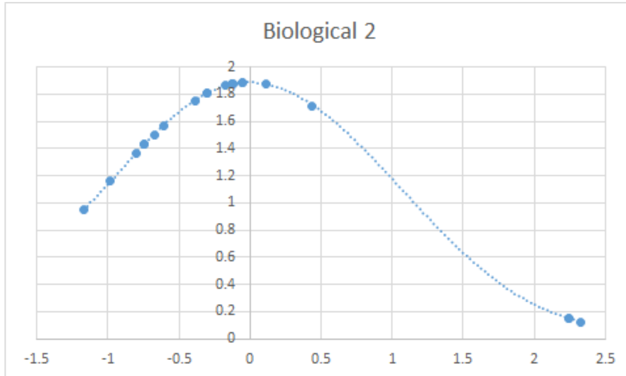

Figure 10: Aerial Biological Object Video Time Interval SND: Sample Two

Standard Deviation Percentage					
μ-3σ	μ-2σ	μ-σ	μ+σ	μ+2σ	μ+3σ
0	1	15	1	0	3
0	0.05	0.75	0.05	0	0.15
0	5	75	5	0	15
		80			
	85				
100					

Figure 11: Aerial Biological Object Time Interval Video Interpretation: Sample Two

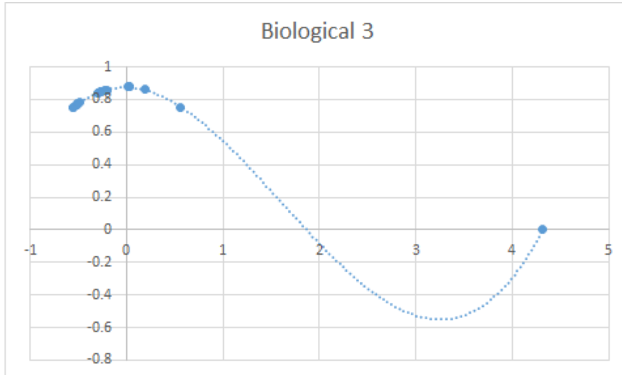

Figure 12: Aerial Biological Object Video Time Interval SND: Sample Three

<table>
<tr><th colspan="6">Standard Deviation Percentage</th></tr>
<tr><td>μ-3σ</td><td>μ-2σ</td><td>μ-σ</td><td>μ+σ</td><td>μ+2σ</td><td>μ+3σ</td></tr>
<tr><td>0</td><td>0</td><td>15</td><td>5</td><td>0</td><td>0</td></tr>
<tr><td>0</td><td>0</td><td>0.75</td><td>0.25</td><td>0</td><td>0</td></tr>
<tr><td>0</td><td>0</td><td>75</td><td>25</td><td>0</td><td>0</td></tr>
<tr><td></td><td></td><td colspan="2">100</td><td></td><td></td></tr>
<tr><td></td><td colspan="4">100</td><td></td></tr>
<tr><td colspan="6">100</td></tr>
</table>

Figure 13: Aerial Biological Object Time Interval Video Interpretation: Sample Three

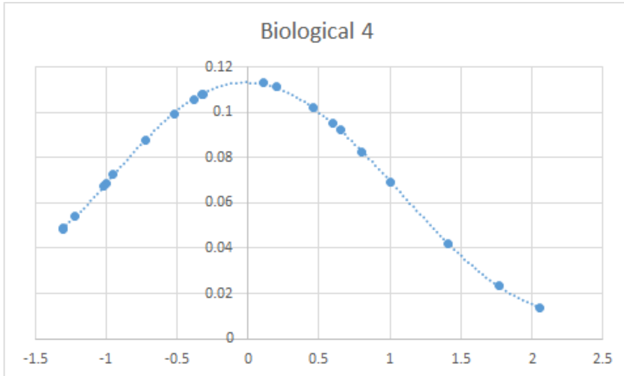

Figure 14: Aerial Biological Object Video Time Interval SND: Sample Four

Standard Deviation Percentage					
μ-3σ	μ-2σ	μ-σ	μ+σ	μ+2σ	μ+3σ
0	5	6	7	2	1
0	0.238095	0.285714	0.333333	0.095238	0.047619
0	23.80952	28.57143	33.33333	9.52381	4.761905
		61.9047619			
	95.23809524				
100					

Figure 15: Aerial Biological Object Time Interval Video Interpretation: Sample Four

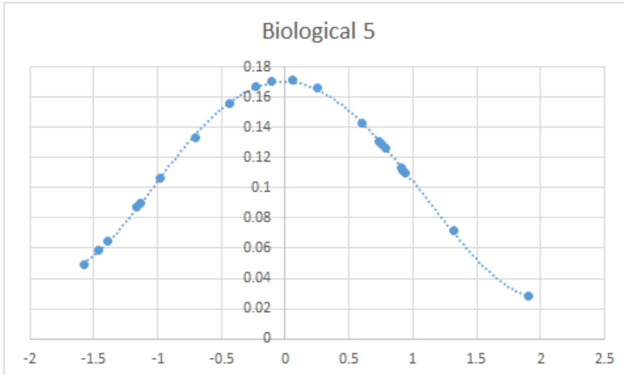

Figure 16: Aerial Biological Object Video Time Interval SND: Sample Five

Standard Deviation Percentage					
μ-3σ	μ-2σ	μ-σ	μ+σ	μ+2σ	μ+3σ
0	5	5	9	2	0
0	0.238095	0.238095	0.428571	0.095238	0
0	23.80952	23.80952	42.85714	9.52381	0
		66.66666667			
	100				
100					

Figure 17: Aerial Biological Object Time Interval Video Interpretation: Sample Five

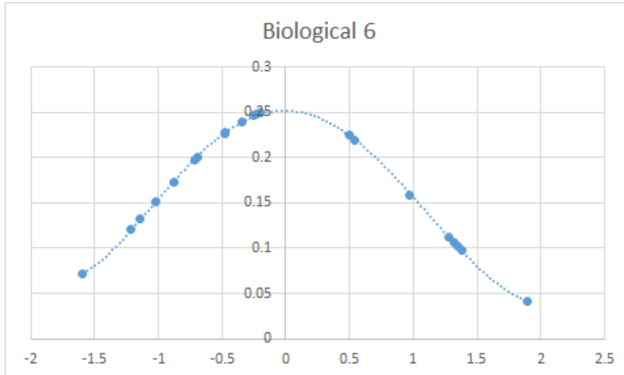

Figure 18: Aerial Biological Object Video Time Interval SND: Sample Six

Standard Deviation Percentage					
μ-3σ	μ-2σ	μ-σ	μ+σ	μ+2σ	μ+3σ
0	4	9	3	5	0
0	0.190476	0.428571	0.142857	0.238095	0
0	19.04762	42.85714	14.28571	23.80952	0
		57.14285714			
	100				
100					

Figure 19: Aerial Biological Object Time Interval Video Interpretation: Sample Six

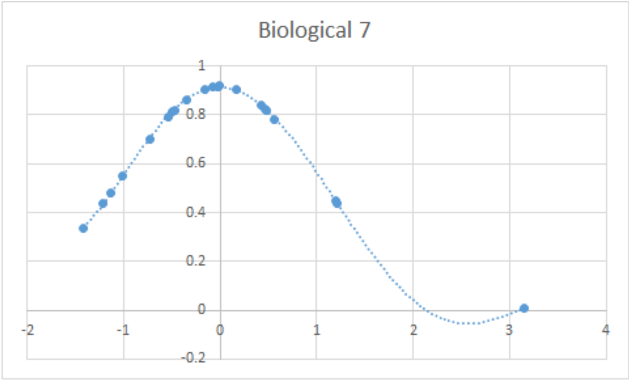

Figure 20: Aerial Biological Object Video Time Interval SND: Sample Seven

Standard Deviation Percentage					
μ-3σ	μ-2σ	μ-σ	μ+σ	μ+2σ	μ+3σ
0	4	9	5	2	0
0	0.2	0.45	0.25	0.1	0
0	20	45	25	10	0
		70			
	100				
100					

Figure 21: Aerial Biological Object Time Interval Video Interpretation: Sample Seven

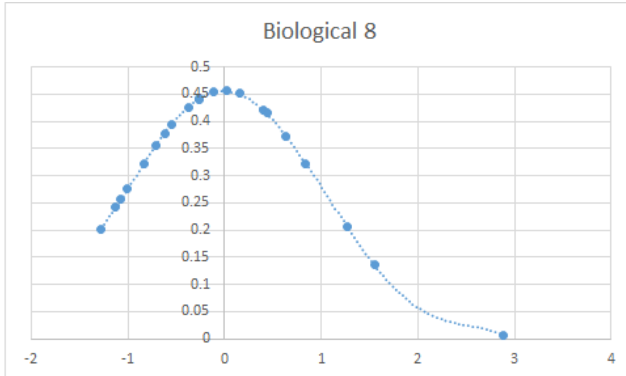

Figure 22: Aerial Biological Object Video Time Interval SND: Sample Eight

Standard Deviation Percentage					
μ-3σ	μ-2σ	μ-σ	μ+σ	μ+2σ	μ+3σ
0	4	8	6	2	1
0	0.190476	0.380952	0.285714	0.095238	0.047619
0	19.04762	38.09524	28.57143	9.52381	4.761905
		66.66666667			
	95.23809524				
100					

Figure 23: Aerial Biological Object Time Interval Video Interpretation: Sample Eight

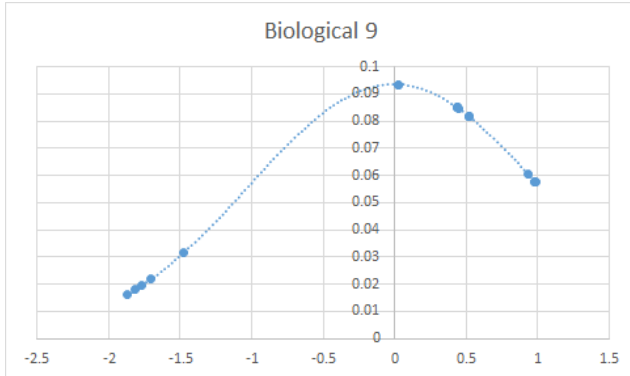

Figure 24: Aerial Biological Object Video Time Interval SND: Sample Nine

Standard Deviation Percentage					
μ-3σ	μ-2σ	μ-σ	μ+σ	μ+2σ	μ+3σ
0	5	0	16	0	0
0	0.238095	0	0.761905	0	0
0	23.80952	0	76.19048	0	0
		76.19047619			
	100				
100					

Figure 25: Aerial Biological Object Time Interval Video Interpretation: Sample Nine

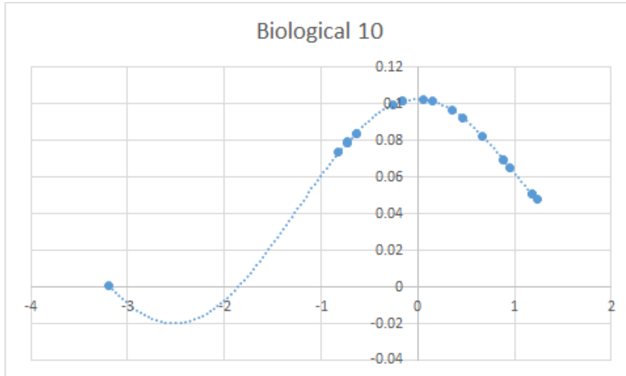

Figure 26: Aerial Biological Object Video Time Interval SND: Sample Ten

Standard Deviation Percentage					
μ-3σ	μ-2σ	μ-σ	μ+σ	μ+2σ	μ+3σ
0	0	9	8	3	0
0	0	0.45	0.4	0.15	0
0	0	45	40	15	0
		85			
	100				
100					

Figure 27: Aerial Biological Object Time Interval Video Interpretation: Sample Ten

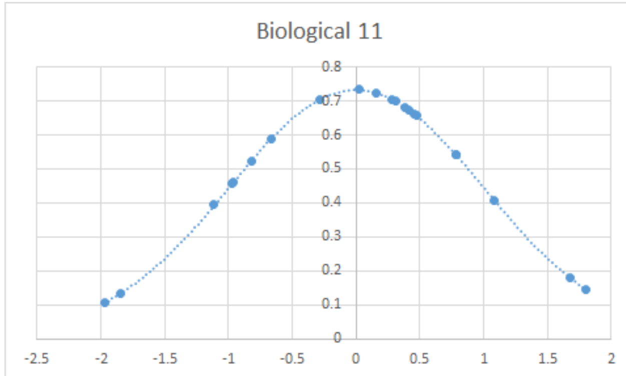

Figure 28: Aerial Biological Object Video Time Interval SND: Sample Eleven

Standard Deviation Percentage					
μ-3σ	μ-2σ	μ-σ	μ+σ	μ+2σ	μ+3σ
0	3	5	10	3	0
0	0.142857	0.238095	0.47619	0.142857	0
0	14.28571	23.80952	47.61905	14.28571	0
		71.42857143			
	100				
100					

Figure 29: Aerial Biological Object Time Interval Video Interpretation: Sample Eleven

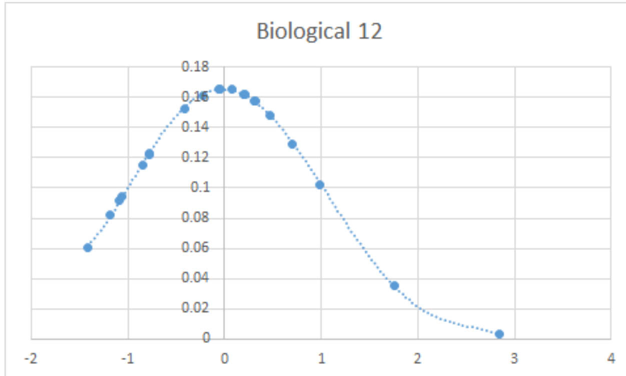

Figure 30: Aerial Biological Object Video Time Interval SND: Sample Twelve

Standard Deviation Percentage					
μ-3σ	μ-2σ	μ-σ	μ+σ	μ+2σ	μ+3σ
0	4	7	8	1	1
0	0.190476	0.333333	0.380952	0.047619	0.047619
0	19.04762	33.33333	38.09524	4.761905	4.761905
		71.42857143			
	95.23809524				
100					

Figure 31: Aerial Biological Object Time Interval Video Interpretation: Sample Twelve

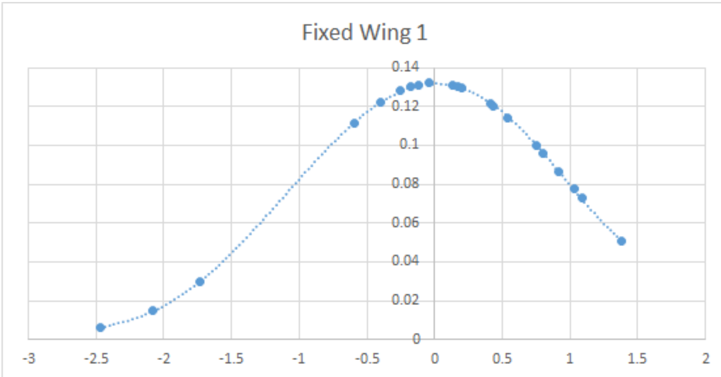

Figure 32: Aerial Manmade (Fixed Wing) Object Video Time Interval SND: Sample One

Standard Deviation Percentage					
μ-3σ	μ-2σ	μ-σ	μ+σ	μ+2σ	μ+3σ
2	1	6	9	3	0
0.0952381	0.047619	0.285714286	0.42857143	0.1428571	0
9.52380952	4.7619048	28.57142857	42.8571429	14.285714	0
		71.42857143			
	90.47619048				
100					

Figure 33: Aerial Manmade (Fixed Wing) Object Time Interval Video Interpretation: Sample One

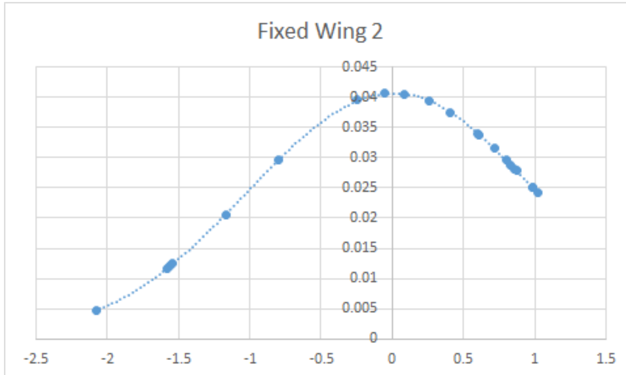

Figure 34: Aerial Manmade (Fixed Wing) Object Video Time Interval SND: Sample Two

Standard Deviation Percentage					
μ-3σ	μ-2σ	μ-σ	μ+σ	μ+2σ	μ+3σ
1	4	3	12	1	0
0.047619	0.190476	0.142857	0.571429	0.047619	0
4.761905	19.04762	14.28571	57.14286	4.761905	0
		71.42857143			
95.23809524					
100					

Figure 35: Aerial Manmade (Fixed Wing) Object Time Interval Video Interpretation: Sample Two

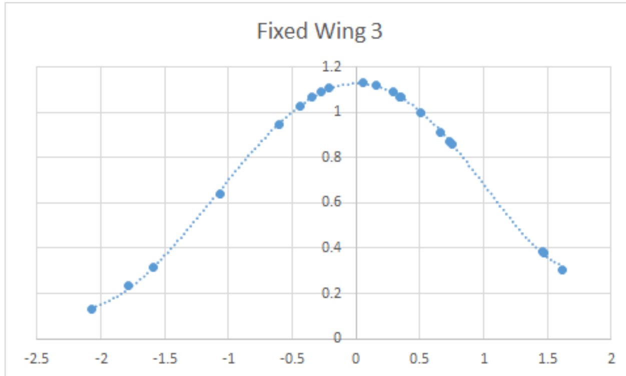

Figure 36: Aerial Manmade (Fixed Wing) Object Video Time Interval SND: Sample Three

Standard Deviation Percentage					
μ-3σ	μ-2σ	μ-σ	μ+σ	μ+2σ	μ+3σ
1	3	5	8	3	0
0.05	0.15	0.25	0.4	0.15	0
5	15	25	40	15	0
		65			
	95				
100					

Figure 37: Aerial Manmade (Fixed Wing) Object Time Interval Video Interpretation: Sample Three

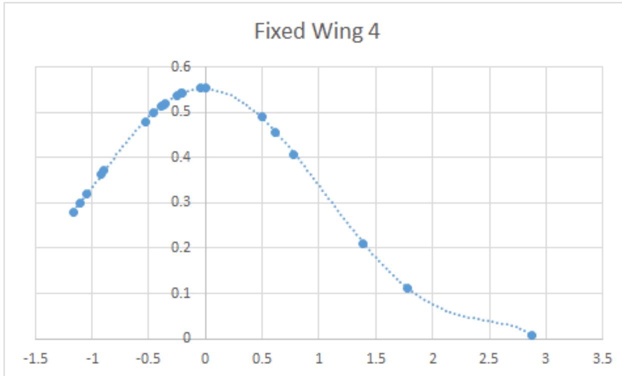

Figure 38: Aerial Manmade (Fixed Wing) Object Video Time Interval SND: Sample Four

Standard Deviation Percentage					
μ-3σ	μ-2σ	μ-σ	μ+σ	μ+2σ	μ+3σ
0	1	11	4	2	1
0	0.052632	0.578947	0.210526	0.105263	0.052632
0	5.263158	57.89474	21.05263	10.52632	5.263158
		78.94736842			
	94.73684211				
100					

Figure 39: Aerial Manmade (Fixed Wing) Object Time Interval Video Interpretation: Sample Four

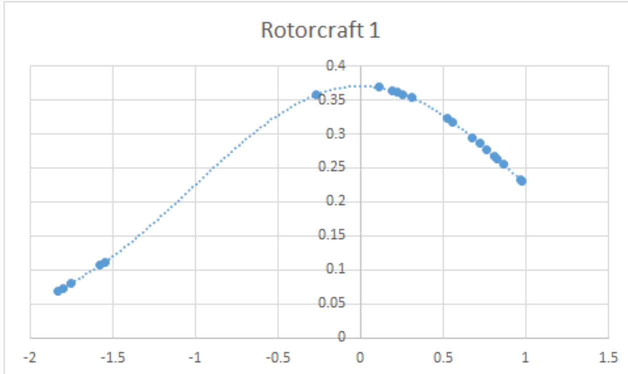

Figure 40: Aerial Manmade (Rotorcraft) Object Video Time Interval SND: Sample One

Standard Deviation Percentage					
μ-3σ	μ-2σ	μ-σ	μ+σ	μ+2σ	μ+3σ
0	5	1	15	0	0
0	0.238095	0.047619	0.714286	0	0
0	23.80952	4.761905	71.42857	0	0
		76.19047619			
	100				
100					

Figure 41: Aerial Manmade (Rotorcraft) Object Time Interval Video Interpretation: Sample One

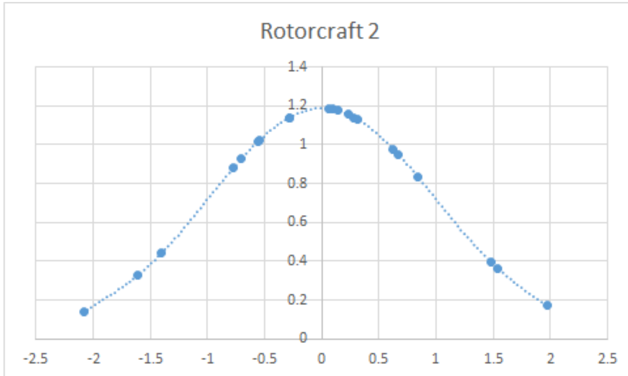

Figure 42: Aerial Manmade (Rotorcraft) Object Video Time Interval SND: Sample Two

Standard Deviation Percentage					
μ-3σ	μ-2σ	μ-σ	μ+σ	μ+2σ	μ+3σ
1	2	6	9	3	0
0.047619	0.095238	0.285714	0.428571	0.142857	0
4.761905	9.52381	28.57143	42.85714	14.28571	0
		71.42857143			
	95.23809524				
100					

Figure 43: Aerial Manmade (Rotorcraft) Object Time Interval Video Interpretation: Sample Two

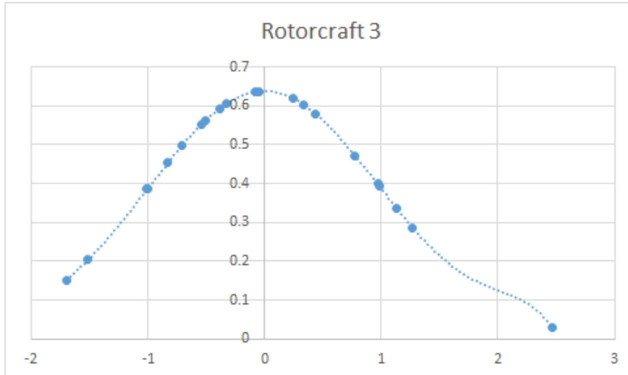

Figure 44: Aerial Manmade (Rotorcraft) Object Video Time Interval SND: Sample Three

Standard Deviation Percentage					
μ-3σ	μ-2σ	μ-σ	μ+σ	μ+2σ	μ+3σ
0	3	9	6	2	1
0	0.142857	0.428571	0.285714	0.095238	0.047619
0	14.28571	42.85714	28.57143	9.52381	4.761905
		71.42857143			
	95.23809524				
100					

Figure 45: Aerial Manmade (Rotorcraft) Object Time Interval Video Interpretation: Sample Three

References

[1] Federal Aviation Administration. Introduction to tcas ii. *Federal Aviation Administration Advisory Circular*, 2011.

[2] Federal Aviation Administration. Interpretation of the special rule for model aircraft. *14 CFR Part 91*, 2012.

[3] Federal Aviation Administration. Public law 112-95, title iii, subtitle b unmanned aircraft systems. *FAA Modernization and Reform ACT of 2012 Public Law*, 2012.

[4] Federal Aviation Administration. Chapter 1, subchapter a, part 1, definitions, civil aircraft, section 1.1. *Title 14 Code of Federal Regulations*, 2016.

[5] Federal Aviation Administration. Chapter 1, subchapter c, part 21, certification procedures for products and parts. *Title 14 Code of Federal Regulations*, 2016.

[6] Russ Tedrake Andrew J. Barry. Pushbroom stereo for high-speed navigation in cluttered environments. *2015 IEEE International Conference on Robotics and Automation (ICRA)*, 2015.

[7] Mark Stout Jason Glaneueski Chris Wargo, Gary Church. Unmanned aircraft system (uas) research and future analysis. *IEEE 978-1-4799-1622-1/14*, 2014.

[8] L. Forlenza A. Moccia D. Accardo, G. Fasano and A. Rispoli. Flight test of a radar-based tracking system for uas sense and avoid. *IEEE Transactions on Aerospace and Electronic Systems*, 49(2), 2013.

[9] Transportation Department and the Federal Aviation Administration. Clarification of the applicability of aircraft registration requirements for unmanned aircraft systems(uas) and request for information regarding electronic registration for uas for uas. *Federal Aviation Administration Notices*, 2015.

[10] D. Tirri A.E. Moccia A. De Lellis E. Fasano G., Accardo. Morphological filtering and target tracking for vision-based uas sense and avoid. *Unmanned Aircraft Systems (ICUAS)*, 2014.

[11] J. D. Bokovi J. A. Jackson and D. Diel. Sensor fusion for sense and avoid for small uas without ads-b. *Unmanned Aircraft Systems (ICUAS)*, 2015.

[12] Johannes Schneider Dirk Holz Thomas Labe Sven Behnke Matthias Nieuwenhuisen, David Droeschel. Multimodal obstacle detection and collision avoidance for micro aerial vehicles. *2013 European Conference on Mobile Robots (ECMR)*, 2013.

[13] Matt Malchano Alex Perkins Alfred A. Rizzi Larry Matthies Max Bajracharya, Jeremy Ma. High fidelity day and night stereo mapping with vegetation and negative obstacle detection for vision-in-the-loop walking. *2013 IEEE RSJ International Conference on Intelligent Robots and Systems (IROS)*, 2013.

[14] Air Traffic Organizations Planning Office of Aviation Research and Development. Literature review on detect, sense, and avoid technology for unmanned aircraft systems. *National Technical Information Service (NTIS)*, 2009.

[15] The White House Office of the Press Secretary. Presidential memorandum: Promoting economic competitiveness while safeguarding privacy, civil rights, and civil liberties in domestic use of unmanned aircraft systems. *Unmanned Aircraft Systems (UAS) Regulations and Policies*, 2015.

[16] U.S. Department of Transportation. N jo 7210.891 unmanned aircraft operations in the national airspace system (nas). *Federal Aviation Administration, Regulations and Policies, Orders and Notices*, 2015.

[17] Shankar Prasad Shibarchi Majumder, Rahul Shankar Mani. Obstacle size and proximity detection using stereo images for agile aerial robots. *2015 2nd International Conference on Signal Processing and Integrated Networks (SPIN)*, 2015.